Calculation of the local optoelectronic properties of nanostructured silicon

A. Mattoni,[1,*] L. Ferraro,[2,†] and L. Colombo[1,3,‡]

[1]*Sardinian Laboratory for Computational Materials Science, SLACS (CNR-INFM), Cittadella Universitaria, I-09042 Monserrato (Ca), Italy*

[2]*Consorzio interuniversitario per le Applicazioni di Supercalcolo Per Università e Ricerca, CASPUR, Via dei Tizii 6b, 00185 Roma, Italy*

[3]*Dipartimento di Fisica Università di Cagliari, Cittadella Universitaria, I-09042 Monserrato (Ca), Italy*

(Received 29 October 2008; published 1 June 2009)

We combine model potential molecular dynamics and tight-binding electronic structure calculations into an order $\mathcal{O}(N)$ theoretical framework to investigate finite-temperature optoelectronic and structural properties of large-scale (10^5 atoms) amorphous-crystalline systems. We prove that the optical absorption is not affected by electron confinement and it varies almost linearly with the crystallinity of the system.

DOI: 10.1103/PhysRevB.79.245302 PACS number(s): 73.22.−f, 07.05.Tp, 61.46.Hk, 81.10.Jt

I. INTRODUCTION

The macroscopic properties of nanostructured materials are governed by the interplay between the local chemical bonding features and the embedding atomic structure. The case of silicon is paradigmatic: though the properties of crystalline silicon (c-Si) are well understood in terms of covalent bonding, the properties of real (i.e., defected, disordered, or nanostructured) systems are not easily predicted because of their structural complexity. There are huge numbers of technologically relevant silicon systems where structural disorder affects the observed properties including: doped, implanted, or even amorphous (a-Si) samples. In particular, a-Si has a larger optical absorption than the c-Si and, therefore, biphasic amorphous-crystalline (a-c) systems (consisting of silicon grains embedded into an amorphous matrix) are currently under investigation for possible applications in low cost optoelectronics and photovoltaics.[1] Similar disordered systems, where nanograins are embedded into layers of amorphous silicon dioxide (silicon carbide or silicon nitride), are promising as well for third generation photovoltaics.[2]

The complex two-phase structure of the a-c material (as well as its tendency to crystallize[1]) makes it quite difficult to predict theoretically the optoelectronic properties of the system, even in the case of elemental silicon. The theoretical challenge is to locally correlate the optoelectronic properties to the actual amount of disorder and to its atomic scale features. In addition, when searching for efficient absorbing layers, the goal is to predict the a-c mixture for which the optical absorption is maximum (in the energy range of interest). This is a twofold open problem: first of all, it is not obvious whether a simple relation can be established between the absorption and the relative abundance of the two phases; furthermore, this calculation is challenging from the methodological and computational point of view. On the one side, it is necessary to generate atomistic models reproducing the rich diversity of a-c morphological features, as well as their microstructure evolution under controlled thermodynamic conditions; on the other hand, the corresponding electronic properties must be computed over a large number of atoms. While the first issue can be coped with large-scale molecular dynamics (MD) simulations based on reliable empirical force fields, the second one does require a much more computer-intensive quantum calculation. This is a major computational bottleneck severely affecting the actual size of the system that can be investigated and, therefore, limiting the pertinence of atomistic models to meet the experimentally observed structural complexity at the nanoscale.

Quite a few linear scaling $\mathcal{O}(N)$ electronic structure methods have been proposed[3,4] typically based on the concept of locality.[5,6] The key idea is that in finite-gap materials several electronic properties only depend on the local environment. $\mathcal{O}(N)$ methods exist for first principles,[7] as well as for empirical tight binding (ETB) (Ref. 8) or pseudopotential[9] calculations. Most applications so far have been focused on ordered structures such as single nanocrystals.[9,10] Very recently, $\mathcal{O}(N)$ first-principles calculations have been applied to organic amorphouslike systems,[11] treating several thousands of atoms. Interesting enough, the structural relaxations and the temperature-induced evolution are not taken into account. In this work we exploit the above concept of localization and we link it to the microstructure evolution of the underlying atomic configuration. To this aim, we develop a $\mathcal{O}(N)$ computational procedure based on a combination of ETB and MD. We apply the present method to investigate local and average optoelectronic properties of very large nanostructured silicon systems and to predict the variation of the optical absorption upon crystallinity.

II. COMPUTATIONAL FRAMEWORK

The simulated system is textured nanocrystalline silicon, as reported in Fig. 1 (center panels) in a y-z view. A typical simulation cell contains 10^5 atoms and it is formed by a distribution of columnar crystalline grains embedded into an otherwise a-Si matrix.[1,12] The evolution of the system is studied by constant temperature, constant volume MD based on the environment-dependent interatomic force field.[13] The number of grains is fixed during the growth (site saturated crystallization[12]) and it corresponds to a constant number density $d_G=\lambda^{-3}$ of crystal seeds ($\lambda \sim 5$ nm). Computational details are reported elsewhere.[1,12] Different configurations are selected during a 3.5-ns-long annealing at $T=1200$ K. Each configuration is characterized in terms of structural and optoelectronic properties.

A. Spatial decomposition

Since the system is nonhomogeneous, we are interested in calculating both the space-resolved (i.e., local) and average

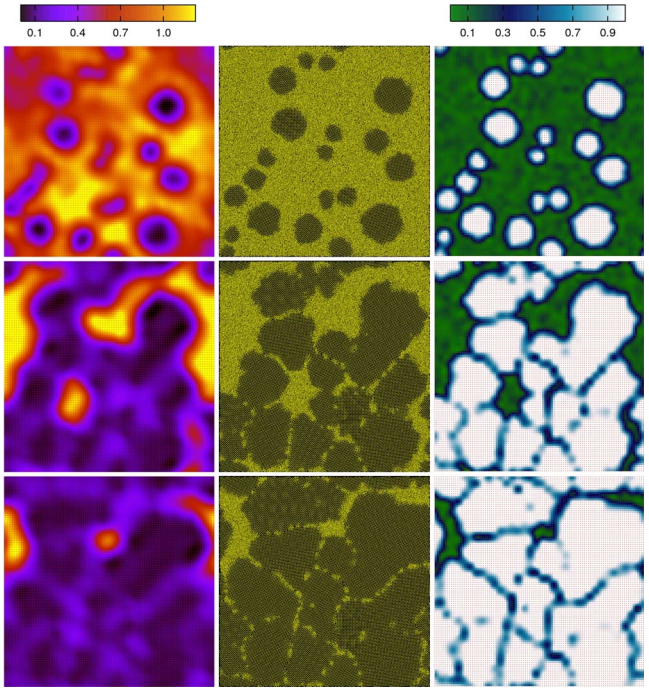

FIG. 1. (Color online) Center: Snapshots of the nc-Si structure at $T=1200$ K at times $t=0.53$ ns (top), $t=0.66$ ns (middle), and $t=1.05$ ns (bottom). Color maps of the local crystallinity $\chi(y,z)$ (right panels) and the local integrated absorption $\Omega(y,z)$ (left panels) are also reported.

properties. To this aim, the whole system of volume W is tessellated by a mesh of $M=m_x\times m_y\times m_z$ nonoverlapping tetragonal cells (hereafter numbered by the upper label α) of size $L_x\times L_y\times L_z$, each containing N^α atoms. Any physical property $P^\alpha(t)$ at time t is calculated in the corresponding αth cell. This is obtained by cutting a cluster $\bar{\alpha}$ of size $\bar{L}_x\times\bar{L}_y\times\bar{L}_z$ formed by the cell itself (the core of the cluster) plus a buffer region of size b. An example is reported in Fig. 2 where the core and the buffer correspond to white and red atoms, respectively.

If a physical property strictly depends only on the local environment (principle of nearsightedness or locality), it can be calculated exactly within α by taking into account only the $\bar{\alpha}$ cluster. For example, the use of a short-range force model for MD is justified in silicon on the basis of the above principle of locality. Within this model, the atomic forces in a cell α are calculated exactly using a buffer $b>R_C$, where R_C is the cutoff for the adopted interaction model.

The same local calculation can be repeated for each α up to completely span the volume W. Once all $P^\alpha(t)$ are known, the average value of the given property can be calculated as $P(t)=M^{-1}\Sigma_{\alpha=1,M}P^\alpha(t)$. Interpolation of local $P^\alpha(t)$ data is also possible by using an spline algorithm (e.g., thin plate spline[14]), so obtaining a continuum field $P(\vec{x},t)$ over W. We will refer hereafter to this computational procedure as divide-and-conquer (DaC), consistently with the literature.[15] It is easy to realize that the corresponding computational workload to calculate $P(t)$ scales linearly with the number of cells and, therefore, it scales linearly with the number of atoms.

The above DaC procedure can be exploited to calculate the electronic properties. In this case the calculated $P^\alpha(t)$ quantities are not exact. Nevertheless, it has been proved recently[5,6] that in finite-gap material the error decreases exponentially with the buffer size. If b is large enough, then the local property $P^\alpha(t)$ can be calculated with an arbitrarily small error by using the cluster $\bar{\alpha}$ instead of the whole system. The size of each cell in the DaC method is chosen so as to fulfill the following requirements: (i) it has to be large enough in order to avoid too large fluctuations of the local observables; (ii) it has to be small with respect to the length scale of the nanostructure (e.g., the grain size) in order to exploit its local character.

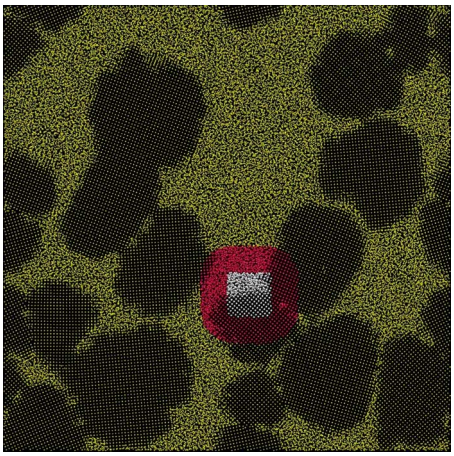

FIG. 2. (Color online) An example of cluster used to calculate the local properties of nanocrystalline silicon. The cluster is formed by the core (white) plus a buffer (red). The buffer is the smallest region with the property that the distance between any point in the core and the external buffer surface is greater than a suitable constant b (buffer size).

B. Calculation of the crystallinity

The local crystallinity χ^α (obtained from the structure factor[1]) was obtained by using a mesh of $1\times35\times35$ cells of dimension $L_x=2.5$ nm$\times L_y=0.72$ nm$\times L_z=0.72$ nm. The corresponding crystallinity maps $\chi(y,z)$ are reported in Fig. 1 (right panels). At each time, a visual comparison with the center panels shows that crystalline grains are accurately reproduced by those regions where $\chi\sim1$.

C. Calculation of the electronic properties

The above DaC approach can be exploited for the calculation of the electronic structure properties as well. We adopt an ETB Hamiltonian[16] with an sp^3s^* basis of $n_b=5$ orbitals for each atom. We develop a DaC procedure in four steps:

Step (i). We divide the system into cells and we calculate the electronic eigenvectors ϵ_i and eigenfunctions $|\psi_i\rangle$ of each corresponding cluster separately (still using the buffer region). We use a mesh of $1\times10\times10$ cells of dimension $5a_0\times5a_0\times5a_0$ (a_0 is the silicon lattice parameter). Periodic boundary conditions are applied along z direction while in y-z plane we fix $b=a_0$. The corresponding number of atoms in each cluster was $\bar{N}^\alpha\sim1800$.

Step (ii). We project the calculated electronic density (and

related quantities) onto the core regions. In particular, we calculate the local density of states $d^{\alpha}(E)$.

Step (iii). The global Fermi level μ is calculated by using the electronic levels of the whole set of M cells. μ is fixed by the condition that the total electronic charge of the system is equal to the total number of valence electrons $4N=4\times10^5$ of the system.

Step (iv). Finally, we calculate the local absorption coefficient $\omega^{\alpha}(E)$ within the constant matrix approximation;[17] accordingly $\omega^{\alpha}(E)\sim E^{-1}j^{\alpha}(E)$, where $j^{\alpha}(E)$ is the local joint density of states,

$$j^{\alpha}(E)=\sum_{E_i\langle\mu,E_j\rangle\mu} d^{\alpha}(E_i)d^{\alpha}(E_j)\,\delta(E_j-E_i-E). \qquad (1)$$

We also calculate the integrated absorption coefficient Ω^{α} such as: $\Omega^{\alpha}=\int_0^{E^{\max}}\omega(E)dE$. In this work we set $E^{\max}=2$ eV, so that Ω^{α} is the average absorption over a range of photon energies close to the band gap and relevant for photovoltaics. The above steps (i)–(iv) were repeated for different choices of the mesh; the corresponding data sets were collected to calculate the final averages and maps. The calculated absorption maps $\Omega(y,z)(t)$ are reported in Fig. 4 (left panels).

We remark that steps (i), (ii), and (iv) are performed independently on each cell and, therefore their computational workload is easily distributed by an embarrassingly parallel scheme. Conversely, step (iii) is possible only after that all local calculations have been performed by collecting the whole set of eigenvalues. At variance with other approaches discussed in the literature,[18] the present one makes it possible to calculate the full set of eigenvectors and eigenfunctions (within the approximation of locality) without storing the whole Hamiltonian matrix into the computer memory. This is beneficial for really large-scale simulations.

D. Numerical accuracy of the DaC method

We focus on the nanocrystalline system reported in Fig. 2. In principle, the calculated electronic properties depend on the buffer size b used in steps (i) and (ii). For the sake of simplicity we consider only the cell α represented in Fig. 2. In order to study the accuracy of the method, the buffer size b is varied in the range $[0.0-3.0]a_0$ and the local electronic properties are calculated accordingly. The buffer represented in Fig. 2 corresponds to the case $b=3a_0$. The absorption coefficient (integrated-absorption coefficient) is calculated as a function of photon energy E and is reported in top (bottom) panel of Fig. 3. Lines correspond to different buffer size b. As the buffer size is increased, the effect of the surface is reduced, and the calculated properties get closer to the correct value that is obtained by including the whole system ($b\to\infty$). For any $b>a_0$ the calculated properties are affected by a negligible error. Sizeable deviations are found only when $b<0.5a_0$. In particular when $b=0$, surface effects are overwhelming and large errors are found (thin black line). The same conclusions are valid for the integrated absorption coefficient (bottom panel), i.e., the quantity we focus on in our work. In this case the convergence is even faster. In particular, using a buffer $b=a_0$, as is the choice we adopted in the work, the local integrated absorption for $E=2$ eV is well reproduced but for an error that is smaller than 3%. When averaged over that whole simulation cell, the error of the integrated absorption becomes even smaller.

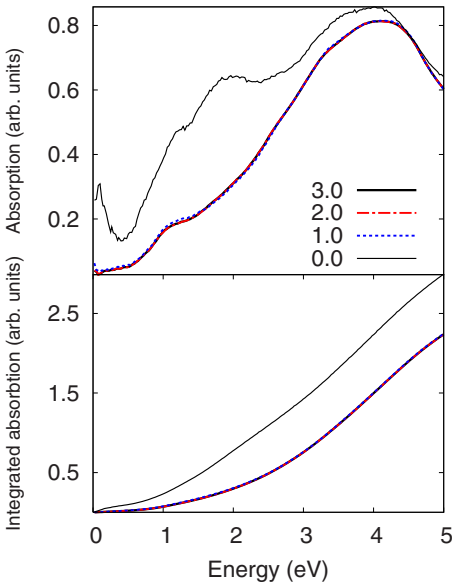

FIG. 3. (Color online) Absorption (top) and integrated absorption (bottom) as a function of the energy E. Lines correspond to different buffer size b (in units of a_0, i.e., the silicon-lattice parameter).

III. RESULTS AND DISCUSSION

The average crystallinity $\chi(t)$ [absorption $\Omega(t)$] depends on time and it is reported in bottom (center) panel of Fig. 4. $\Omega(t)$ decreases during the annealing as the amorphous phase

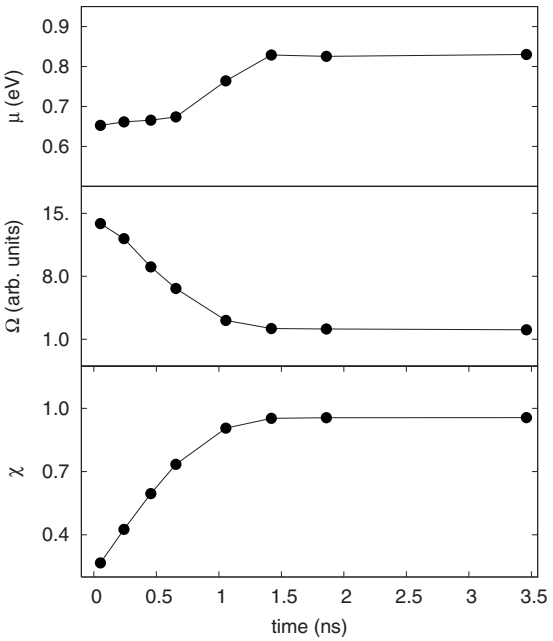

FIG. 4. Time evolution of crystallinity (bottom), integrated absorption (center), and Fermi level (top) during annealing.

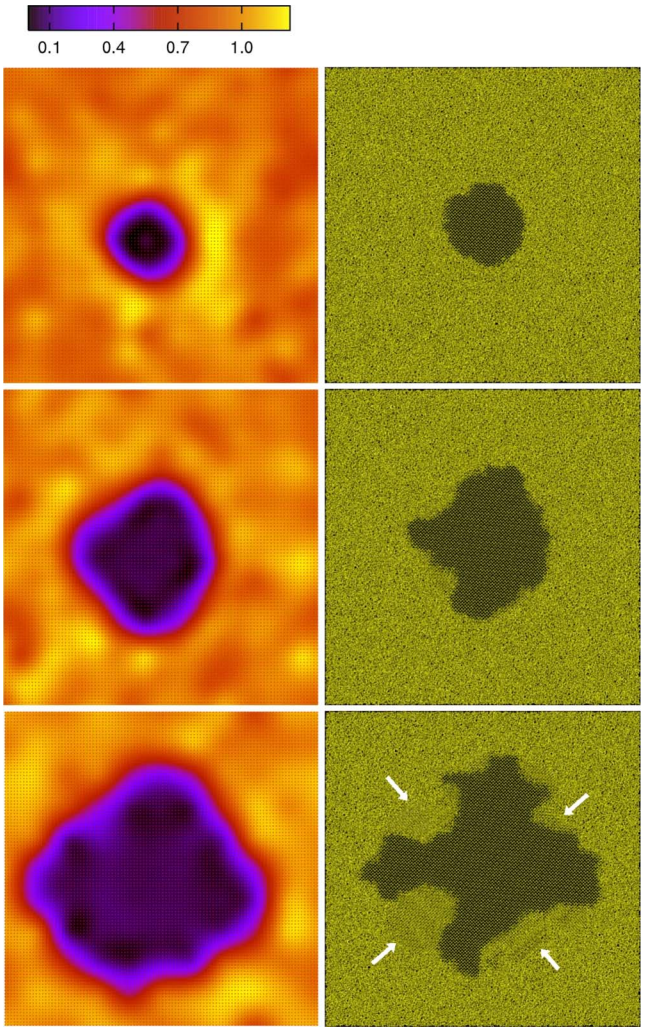

FIG. 5. (Color online) Faceted growth of an embedded nc-Si grain during an isothermal annealing at $T=1200$ K. Morphology (right panel) and integrated absorption map $\Omega(y,z)$ (left panels) are reported at times $t=0.20$ ns, $t=1.39$ ns, and $t=3.2$ ns.

disappears. This result is due to intragap electronic levels in the amorphous phase that are associated to topological defects[19] (Urbach tails) and to angular distortions,[20] as well as to coordination defects. As the system crystallizes and structural order is recovered, the intragap levels disappear and the integrated absorption accordingly decreases as proved by the increasing Fermi level (Fig. 4, top). A comparison between Ω (Fig. 1, left) and χ (Fig. 1, right) shows an overall correlation between local order and local absorption. In particular, lower values of Ω are observed in the core of grains. Nevertheless, at variance with χ, the absorption Ω is quite inhomogeneous within the amorphous phase. Fluctuations are observed within the nanograins as well. Both features are likely due to local residual strain (further discussed below). As for grain size effects, we observe that the absorption of smaller grains is larger and closer to the average a-Si value. This effect is due to a larger surface-to-volume ratio and to a larger number of electronic levels associated to the a-c interface.[20] Furthermore the local electronic gap is practically independent of the grain size.[20]

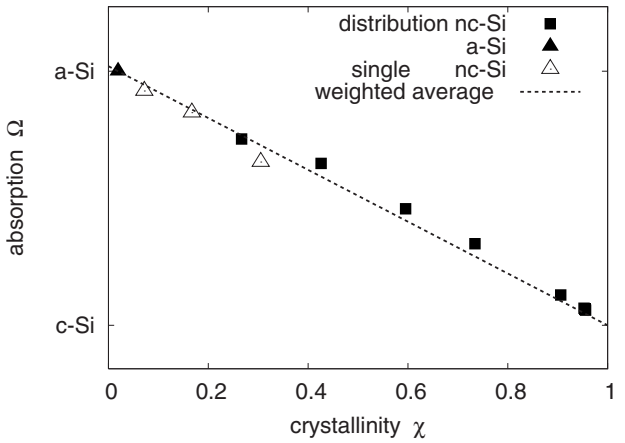

FIG. 6. Integrated absorption Ω vs crystallinity χ during the site saturated crystallization of nanocrystalline silicon at $T=1200$ K. The calculated data for the a-nc phase (squares) and bulk a-Si phase (circle) are compared with LCIA (dashed line).

This result does not support the occurrence of an effective electron confinement in embedded nanograins.

Elsewhere we reported the spontaneous formation of twin boundaries during crystallization.[1] Twins form at the grain facets (marked by arrows in Fig. 5) and affect the grain shape. The chemical bonding of the twin boundaries (up to the first neighbors of atoms) is unchanged with respect to c-Si; accordingly, the optoelectronic properties within crystals containing twins are practically unaffected (Fig. 5, left).

Finally, we calculated the average absorption Ω as a function of the actual crystallinity χ, as reported in Fig. 6 (full squares). Let $\Omega_c(\Omega_a)$ be the integrated absorption in bulk c-Si (a-Si) at the same temperature. We define the linear combination of the integrated absorption (LCIA) as

$$L\Omega(\chi) = \chi\Omega_c + (1-\chi)\Omega_a \tag{2}$$

corresponding to the dashed line of Fig. 6. It is observed that the absorption of the mixed nc-Si phase can be nicely described by Eq. (2). This is true for the case of an isolated grain (open symbols), as well as of nc-Si (full squares). This suggests that the optical absorption of the nc-Si system indeed corresponds to a simple LCIA linear combination of the amorphous and crystalline phases.

We could refine the above picture by observing that it exists a small enhancement of $\Omega(\chi)$ with respect to LCIA in the range $0.4<\chi<0.8$. This feature cannot be linked to the increase in a-c or grain boundaries occurring during grains growth. As a matter of fact, the largest absorption (Fig. 1) is observed within the amorphous phase (yellow regions in Fig. 1 left panels) and not at the a-c or grain boundaries. The above deviations from LCIA are most likely due to the strain locally induced in the amorphous phase by the grains, as predicted by continuum elasticity.[21] In the present case, the stiffer nanograin gives rise to tensile strain in the amorphous matrix. This effect can be clearly observed in Fig. 5, where the absorption of the amorphous matrix is enhanced close to the nanograin (yellow regions). Finally, we remark that when the system is almost completely crystallized ($\chi>0.9$), Ω includes a contribution from the grain boundaries. This contri-

bution is slightly larger than Ω_c (light blue regions, Fig. 1 left bottom panels) while it is much smaller than Ω_a.

In conclusion, by using an empirical $\mathcal{O}(N)$ theoretical framework, we proved that it is possible to study structural and optoelectronic properties of large-scale models (10^5 atoms) of textured nanocrystalline silicon during thermal annealing. We found that the absorption properties of the nanocrystalline phase do not strongly deviate from a simple linear combination between c-Si and a-Si phases and it is not affected by electron confinement within grains. Only a small enhancement is possible, which is attributed to the strain in the amorphous phase.

ACKNOWLEDGMENTS

This work was funded by EU-STREP "NANOPHOTO," MIUR-PON "CyberSar," and "Fondazione Banco di Sardegna" projects. CINECA and CASPUR are also acknowledged for computational support.

*alessandro.mattoni@dsf.unica.it
†l.ferraro@caspur.it
‡luciano.colombo@dsf.unica.it

[1] A. Mattoni and L. Colombo, Phys. Rev. Lett. **99**, 205501 (2007).
[2] G. Conibeer, M. Green, E. C. Cho, D. Konig, Y. H. Cho, T. Fangsuwannarak, G. Scardera, E. Pink, Y. Huang, and T. Puzzer, Thin Solid Films **516**, 6748 (2008).
[3] S. Goedecker, Rev. Mod. Phys. **71**, 1085 (1999).
[4] P. Ordejón, Comput. Mater. Sci. **12**, 157 (1998).
[5] W. Kohn, Phys. Rev. Lett. **76**, 3168 (1996).
[6] E. Prodan and W. Kohn, Proc. Natl. Acad. Sci. U.S.A. **102**, 11635 (2005).
[7] L.-W. Wang, Phys. Rev. Lett. **88**, 256402 (2002).
[8] L. Colombo, Riv. Nuovo Cimento **28**, 1 (2005).
[9] L.-W. Wang and A. Zunger, J. Chem. Phys. **100**, 2394 (1994).
[10] G. Allan, C. Delerue, and M. Lannoo, Phys. Rev. B **57**, 6933 (1998).
[11] N. Vukmirović and L.-W. Wang, J. Chem. Phys. **128**, 121102 (2008).
[12] A. Mattoni and L. Colombo, Phys. Rev. B **78**, 075408 (2008).
[13] M. Z. Bazant, E. Kaxiras, and J. F. Justo, Phys. Rev. B **56**, 8542 (1997).
[14] S. N. Wood, J. Roy. Statist. Soc. Ser. B. Methodological **65**, 95 (2003).
[15] W. Yang, Phys. Rev. Lett. **66**, 1438 (1991).
[16] P. Vogl, H. Hjalmarson, and J. Dow, J. Phys. Chem. Solids **44**, 365 (1983).
[17] F. Bassani and G. P. Parravicini, *Electronic States and Optical Transitions in Solids* (Pergamon Press, Oxford, 1975).
[18] S. Goedecker and L. Colombo, Phys. Rev. Lett. **73**, 122 (1994).
[19] Y. Pan, F. Inam, M. Zhang, and D. A. Drabold, Phys. Rev. Lett. **100**, 206403 (2008).
[20] L. Bagolini, A. Mattoni, and L. Colombo, Appl. Phys. Lett. **94**, 053115 (2009).
[21] P. L. Palla, S. Giordano, and L. Colombo, Phys. Rev. B **78**, 012105 (2008).